Dyes and Pigments 112 (2015) 201–209

Contents lists available at ScienceDirect

Dyes and Pigments

journal homepage: www.elsevier.com/locate/dyepig

A two fluorophore embedded probe for collective and ratiometric detection of Hg^{2+} and F^- ions

Narendra Reddy Chereddy [a, b, *], Peethani Nagaraju [b], M.V. Niladri Raju [b], Krishnan Saranraj [a], Sathiah Thennarasu [a, *], Vaidya Jayathirtha Rao [b, *]

[a] Organic Chemistry Division, CSIR-Central Leather Research Institute, Adyar, Chennai 600 020, India
[b] Crop Protection Chemicals Division, CSIR-Indian Institute of Chemical Technology, Tarnaka, Hyderabad 500 007, India

ARTICLE INFO

Article history:
Received 15 May 2014
Received in revised form
2 July 2014
Accepted 3 July 2014
Available online 15 July 2014

Keywords:
Rhodamine-fluorescein dyad
Hg^{2+} chemosensors
F^- chemosensors
Ratiometric sensors
Live cell imaging
Naked eye detection

ABSTRACT

A novel fluorescein-rhodamine dyad probe has been synthesized and its chemosensory applications are explored. Anion and cation specific responses of the probe permit ratiometric detection of Hg^{2+} and fluoride ions, individually and collectively, with different fluorescence outputs. The presence of other commonly coexistent ions does not affect the Hg^{2+} and fluoride ion detection ability of the probe. The probe is highly sensitive to Hg^{2+} and fluoride ions and it can detect Hg^{2+} and fluoride ions even at ppb level concentrations. The probe is non-toxic under the experimental conditions, cell permeable and useful for the imaging of intracellular Hg^{2+} and fluoride ions.

1. Introduction

Development of fluorescent probes for the selective detection of toxic ions is a developing area of research [1–3]. Mercury is one of the most toxic transition metal ions, and can easily pass through biological membranes [4]. On the other hand, fluoride plays a vital role in the treatment of osteoporosis and in the prevention of dental caries [5–7]. However, exposure to excess levels of fluoride can lead to dental or skeletal fluorosis, or cancer [8–10]. Hence, design, synthesis and evaluation of fluorescent probes with high sensitivity and selectivity toward Hg^{2+} and F^- are highly desirable. Desulfation followed by cyclization reaction of thiourea has been widely exploited for the development of Hg^{2+} selective chemodosimeters [11–19]. Fluoride ion selective cleavage of Si–O linkage has been extensively applied for designing fluoride selective chemosensors [20–26]. Chemosensors suitable for simultaneous detection of multiple analytes are of particular importance for routine analysis in the field or contaminated site. Recently, extensive interest has been devoted by researchers to develop multianalyte chemosensors [27–37]. However, only two systems are available for individual detection of both Hg^{2+} and F^- ions in aqueous samples [29,30]. Considering the extreme toxicity of Hg^{2+} and F^- ions and non-availability of adequate chemosensors, it is imperative to develop new fluorescent probes for individual and collective detection of Hg^{2+} and F^- ions in aqueous and biological samples.

In continuation to our research in the development of fluorescent probes for selective detection of specific metal ions [38–44], we report, herein, a two-fluorophore-embedded fluorescent probe **1**, for simultaneous detection of Hg^{2+} and F^- ions. Selective complexation of Hg^{2+} with the thiourea moiety and F^- promoted cleavage of silyl ether bond, induce cation and anion specific absorption and fluorescence properties. Consequently, ratiometric detection of Hg^{2+} and F^- ions in aqueous samples were evaluated. Selective detection of Hg^{2+} and F^- ions was also examined in the presence of other competing ions. Cytotoxicity of the probe was assessed using MTT assay. To our knowledge, probe **1** is the first of

* Corresponding authors. Organic Chemistry Division, CSIR-Central Leather Research Institute, Adyar, Chennai 600 020, India. Tel.: +91 44 24913289; fax: +91 44 24911589.
E-mail addresses: chereddynarendra@gmail.com (N.R. Chereddy), thennarasu@gmail.com (S. Thennarasu).

http://dx.doi.org/10.1016/j.dyepig.2014.07.004
0143-7208/

its kind that can be used for the simultaneous and ratiometric detection of both Hg^{2+} and F^- ions in both aqueous and biological systems.

2. Experimental section

2.1. General

Dry acetonitrile and double distilled water were used in all experiments. All the materials for synthesis were purchased from commercial suppliers and used without further purification. The W138 (normal lung fibroblast) cells were obtained from American Type Culture Collection (Manassas, VA). Dulbecco's Modified Eagle Medium (DMEM), Dulbecco's Phosphate Buffered Saline (DPBS), Hank's Balanced Salt Solution (HBSS), Fetal Bovine Serum (FBS) and penicillin/streptomycin were purchased from Sigma–Aldrich, USA. The solutions of metal ions were prepared from their corresponding chloride salts and anion solutions were prepared from their corresponding Na or K salts. Absorption spectra were recorded on a Cary 5000 UV-Vis-NIR spectrophotometer. All the absorption measurements were conducted using double beam UV–Visible spectrophotometer and the aqueous acetonitrile system (1:1 v/v 0.01 M Tris HCl–CH_3CN, pH 7.4) was used as blank to correct the influence of common invariants. Fluorescence measurements were performed on a Cary Eclipse fluorescence spectrophotometer (Excitation wavelength 480 nm; excitation, emission slit widths were 5 nm each). All pH measurements were made with a Systronics μpH System Model 361. NMR spectra were recorded using a Bruker 400 and Jeol 500 MHz NMR spectrometers. ESI-High Resolution Mass Spectrum (HRMS) was recorded on QSTAR XL Hybrid MS/MS mass spectrometer. All measurements were carried out at room temperature. Stock solution of the probe was prepared by dissolving 10.73 mg of **1** in 1:1 v/v 0.01 M Tris HCl–CH_3CN (pH 7·4) and making up to the mark in a 10 mL volumetric flask. Further dilutions were made to prepare 5 μM solutions for the experiments. Stock solutions of metal ions and anions (1 M) were prepared in de-ionised water.

2.2. Synthesis of probe *1*

The probe **1** was synthesized in a three-step pathway by reacting rhodamine with hydrazine hydrate, and subsequently the rhodamine hydrazide with fluorescein isothiocyanate (FITC) followed by the protection of hydroxyl groups of fluorescein using TBDMSi-Cl.

2.2.1. Synthesis of intermediate *A*

Rhodamine hydrazide was synthesized as per our previous reported procedure [38].

2.2.2. Synthesis of intermediate *B*

To a solution of rhodamine hydrazide (0.46 g, 1.0 mmol) in DMF (10 mL) fluorescein isothiocyanate (FITC, 0.39 g, 1.0 mmol) was added, and the resultant mixture was stirred overnight at room temperature. After the complete consumption of the starting materials as monitored through TLC, the reaction mixture was purified using silica gel (200–400 mesh, 40:60 ethyl acetate–hexane as eluent) column chromatography to obtain **B** as an orange-red solid (0.45 g, 0.53 mmol, 53% yield).

^{1}H NMR (400 MHz, CD_3OD, δ ppm): 1.042 (t, J = 7.5 Hz, 12H, $NCH_2\underline{CH_3}$), 3.256 (m, 12H, $N\underline{CH_2}CH_3$, 2 NH, COOH, OH), 6.274 (d, J = 7.6 Hz, 2H, Ar-H), 6.416–6.476 (m, 5H, Ar-H), 6.510 (s, 1H, Ar-H), 6.532 (s, 1H, Ar-H), 6.607 (d, J = 2.3 Hz, 2H, Ar-H), 6.901 (d, J = 8.2 Hz, 1H, Ar-H), 7.207 (d, J = 7.6 Hz, 1H, Ar-H), 7.309 (d, J = 8.2 Hz, 1H, Ar-H), 7.597–7.615 (m, 2H, Ar-H), 7.640–7.690 (m, 1H, Ar-H), 7.903–7.971 (m, 1H, Ar-H). ^{13}C NMR (100 MHz, CD_3OD, δ ppm): 11.59, 29.34, 30.30, 35.61, 44.03, 67.88, 97.23, 102.18, 104.43, 108.04, 110.07, 112.27, 112.37, 123.11, 123.48, 124.53, 127.10, 128.83, 129.91, 133.92, 140.32, 149.30, 149.97, 152.79, 154.58, 160.17, 163.50, 167.41, 169.50, 182.93.

2.2.3. Synthesis of rhodamine-fluorescein dyad probe *1*

To a solution of **B** (0.30 g, 0.35 mmol) and imidazole (0.05 g, 0.72 mmol) in DCM (20 mL), *tert*-butyldimethylsilyl chloride (TBDMSi-Cl, 0.12 g, 0.80 mmol) was added, and the resultant mixture was stirred under nitrogen atmosphere for ~6 h and then purified using preparative TLC (using pre-coated alumina plates and hexane-ethyl acetate (80:20) mixture as eluent) to obtain **1** as an orange-yellow solid (0.16 g, 0.15 mmol, 47% yield).

^{1}H NMR (500 MHz, $CDCl_3$, δ ppm): 0.212 (s, 12H, Si–$\underline{CH_3}$), 0.974 (s, 18H, Si–C–$\underline{CH_3}$), 1.164 (t, J = 7.5 Hz, 12H, $NCH_2\underline{CH_3}$), 3.370 (q, J = 7.0 Hz, 8H, $N\underline{CH_2}CH_3$), 6.360 (dd, J = 2.5 Hz, 2H, Ar-H), 6.450–6.540 (m, 6H, Ar-H), 6.560 (s, 1H, Ar-H), 6.581 (s, 1H, Ar-H), 6.690 (d, J = 2.5 Hz, 2H, Ar-H), 6.995 (d, J = 7.5 Hz, 1H, Ar-H), 7.080 (s, 1H, Ar-H), 7.316 (d, J = 7.5 Hz, 1H, Ar-H), 7.399 (s, 1H, Ar-H), 7.609 (t, J = 7.5 Hz, 1H, Ar-H), 7.685 (t, J = 7.5 Hz, 1H, Ar-H), 7.743 (s, 1H, Ar-H), 7.839 (d, J = 8.5 Hz, 1H, Ar-H), 8.024 (d, J = 7.5 Hz, 1H, Ar-H). ^{13}C NMR (125 MHz, $CDCl_3$, δ ppm): − 4.41, − 4.40, 12.57, 18.21, 25.61, 29.70, 44.52, 67.37, 83.04, 98.39, 103.98, 107.62, 108.42, 111.96, 114.08, 116.58, 119.60, 123.71, 123.93, 124.86, 127.16, 127.56, 128.97, 129.18, 131.76, 134.47, 139.29, 139.54, 149.53, 150.05, 150.19, 152.25, 154.41, 157.57, 167.20, 168.46, 182.80. ESI-HRMS: Calcd. for $C_{61}H_{71}N_5O_7SSi_2$ 1073.46127; m/z found 1074.46693 ($M + H^+$).

2.3. Sample preparation for cell culture

Freshly prepared stock solutions of each sample were used for cell culture experiments. A stock solution (10 mM) of **1** was prepared in sterile DMSO. Similarly, 10 mM stock solutions of Hg^{2+} and F^- salts were prepared in sterile Millipore water.

2.4. Cell culture experimentation

W138 and NIH 3T3 cells were maintained in DMEM complete media, supplemented with 10% Fetal Bovine Serum (FBS) and 1% penicillin/streptomycin at 37 °C in a humidified incubator equilibrated with 5% CO_2. Cells showing 70% confluence were seeded into 96-well and 24-well plates for cytotoxicity and fluorescence microscopy studies, respectively.

2.5. MTT assay

The MTT (3-(4,5-dimethylthiazol-2-yl)-2,5-diphenyl tetrazolium bromide) assay has been used to measure the activity of enzymes that reduce MTT to formazan dyes, giving rise to a purple colour. Briefly, about 10,000 NIH 3T3 cells were seeded into each well of a 96-well tissue culture plate containing complete DMEM medium (100 μL) and incubated for 24 h at 37 °C in a humidified incubator equilibrated with 5% CO_2. Next day, the medium in each well was replaced with fresh DMEM medium (100 μL), and the cells were incubated with different concentrations (0.1–10 μM) of probe **1** for 48 h. A 1.0 mL MTT stock solution (5 mg/mL) was diluted to 10 mL using complete DMEM medium, and 100 μL of the diluted MTT solution was added to each well of 96-well plate after replacing the old medium and allowed to incubate for 4 h. After that, the medium in each well was replaced by 100 μL of 1:1 (v/v) DMSO-methanol mixture for solubilizing the purple formazan product. Then, the plate was kept on a shaker to homogenize the solution. Finally, the microplate reader (ELx 800 MS) was used to

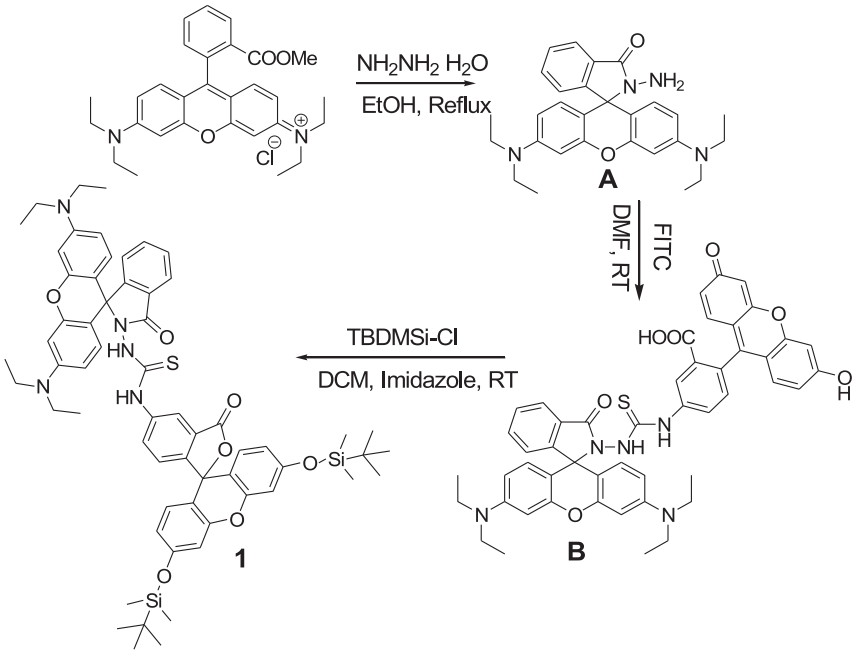

Scheme 1. Synthesis of fluorescein-rhodamine dyad **1.**

measure the absorbance at 570 nm of the solutions in each well of the plate.

2.6. Fluorescence microscopy

To conduct live-cell imaging experiments, W138 cells were seeded at 2×10^4 cells/mL/well in complete DMEM media in a 24-well tissue culture plate and incubated for 24 h at 37 °C in a humidified incubator equilibrated with 5% CO_2. After 24 h, the cells were incubated with probe **1** (5 μM) for another 4 h. The cells were thoroughly washed six times with DPBS to remove the unbound probe **1** from the surface of cell membrane. After that, the cells treated with probe **1** were separately incubated with F^- (50 μM) and Hg^{2+} (5 μM) for 15 min and again washed six times with DPBS to remove the unbound materials. Finally, the fluorescence images of W138 cells alone, cells treated with only probe **1**, cells treated with probe **1** and F^-, and cells treated with probe **1** and Hg^{2+} were observed under fluorescence microscope (Leica DM IRB microscope equipped with EBQ-100 UV-lamp) through the green (Emission filter LP 515) and red (Emission filter LP 590) channels, respectively.

3. Results and discussion

Probe **1** was synthesized in a three-step path way (Scheme 1). Rhodamine hydrazide, prepared as described earlier [38] was reacted with fluorescein isothiocyanate (FITC) and, subsequently, the hydroxyl groups of fluorescein moiety were protected using TBDMSi-Cl to obtain probe **1**, whose formation was confirmed using NMR and ESI-HRMS analyses (Figs. S1–S5, Supporting data). The non-fluorescent nature of probe **1** (5 μM) in aqueous acetonitrile (1:1 v/v 0.01 M Tris HCl–CH_3CN, pH 7.4) was readily observed from its quantum yield (Φ = 0.005 and 0.008, from fluorescein and rhodamine moieties, respectively). The very low Φ values suggested that both fluorescein and rhodamine moieties of probe **1** were in the spirocyclic form.

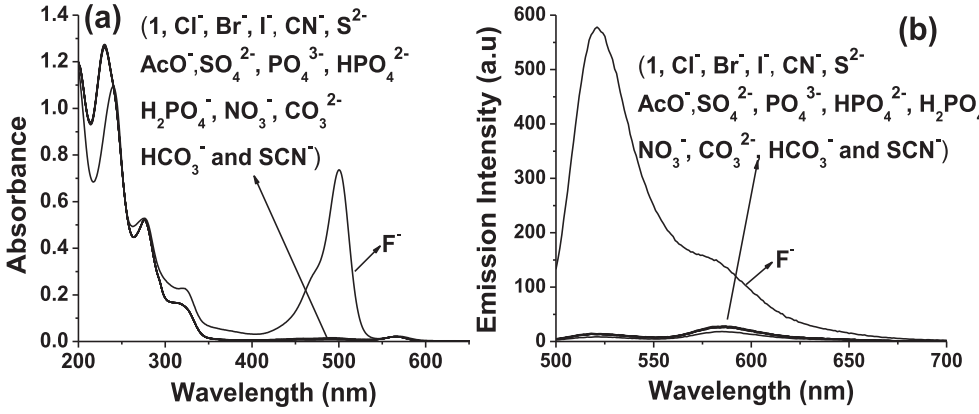

Fig. 1. Anion (150 μM) induced variations in the (a) absorbance, and (b) fluorescence spectra of **1** (5 μM); Excitation wavelength: 480 nm.

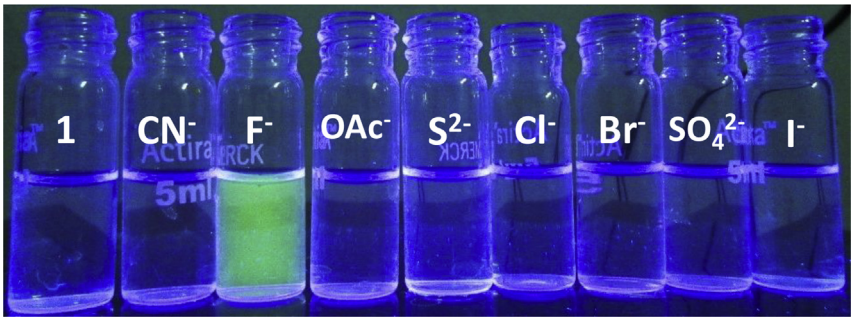

Fig. 2. Naked eye detection of F^- using probe **1**: The effect of the addition of various anions (150 μM) on the fluorescence emission of **1** (5 μM).

We then investigated the effects of Hg^{2+} and F^- ions as well as other competing ions on the absorbance and fluorescence characteristics of **1**. Among the anions (150 μM) added, only fluoride ion triggered a significant increment in the absorbance ($\varepsilon = 148{,}400\ M^{-1}\ cm^{-1}$, Fig. 1a) and fluorescence ($\Phi = 0.26$, Fig. 1b) profiles of **1**. This F^- specific response of **1** could be attributed to the fluoride induced cleavage of Si–O linkage leading to the generation of **2** (Scheme S1, Supporting data), whose formation was confirmed using ESI-MS analysis ($m/z = 846$, Fig. S6, Supporting data). Also, the fluoride selective 'turned-on' green fluorescence emission (Fig. 2) from **1**, enabled naked eye detection of fluoride ions.

In a similar experiment with metal ions, probe **1** (5 μM) remained passive to the addition of different metal ions (15 μM) except Hg^{2+}, whose addition invoked an enhancement in the absorbance (237,600 $M^{-1}\ cm^{-1}$, Fig. 3a) and fluorescence ($\Phi = 0.31$, Fig. 3b) profiles of the rhodamine moiety in **1**, and thereby, enabled the detection of Hg^{2+} with naked eye (Fig. 4). These observations established the reaction based detection of Hg^{2+} ions, and could be attributed to Hg^{2+} induced desulfation and cyclization reaction of the thiourea moiety (Scheme S1, Supporting data) leading to the formation of **3** ($m/z = 1041$, Fig. S7, Supporting data).

To determine the detection limits of the probe [45], changes in absorption and emission characteristics of **1** (5 μM) with different amounts of F^- and Hg^{2+} ions were measured. Addition of F^- (5 μM) provoked new peaks at ~500 and ~523 nm, respectively, in the excitation and emission spectra of **1**. The absorption and emission intensities were increased with the amount of F^- added, and reached the maximum upon addition of 30 equivalents of F^- (Fig. S8, Supporting data). Under similar conditions, addition of 0.5 μM Hg^{2+} developed an excitation band with λ_{max} at ~568 nm and an emission band with λ_{max} at ~592 nm. The intensity of these bands increased gradually with the amount of Hg^{2+} added, and attained the maximum on addition of 2.5 equivalents of Hg^{2+} (Fig. S9, Supporting data). Thus, the absorption and emission

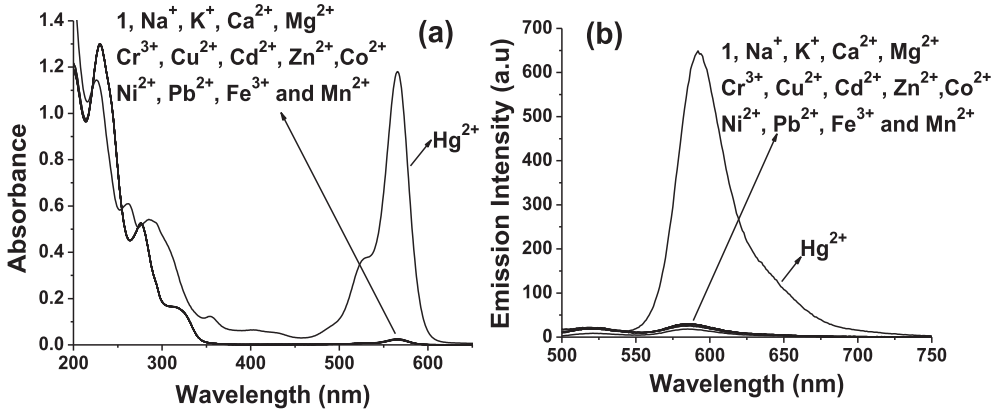

Fig. 3. Metal ion (15 μM) induced variations in the (a) absorbance, and (b) fluorescence spectra of **1** (5 μM); Excitation wavelength: 480 nm.

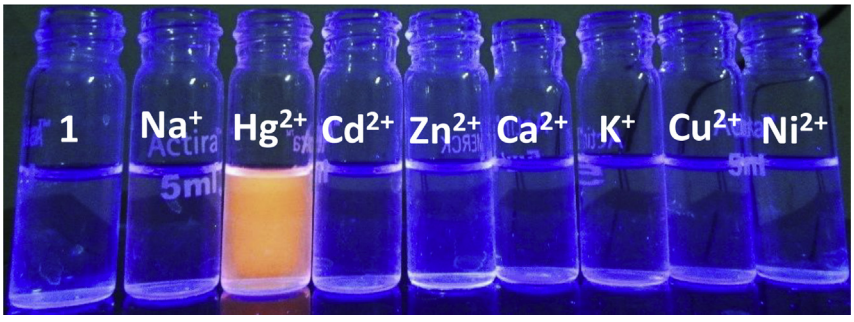

Fig. 4. Naked eye detection of Hg^{2+} using probe **1**: The effect of the addition of various metal ions (15 μM) on the fluorescence emission of **1** (5 μM).

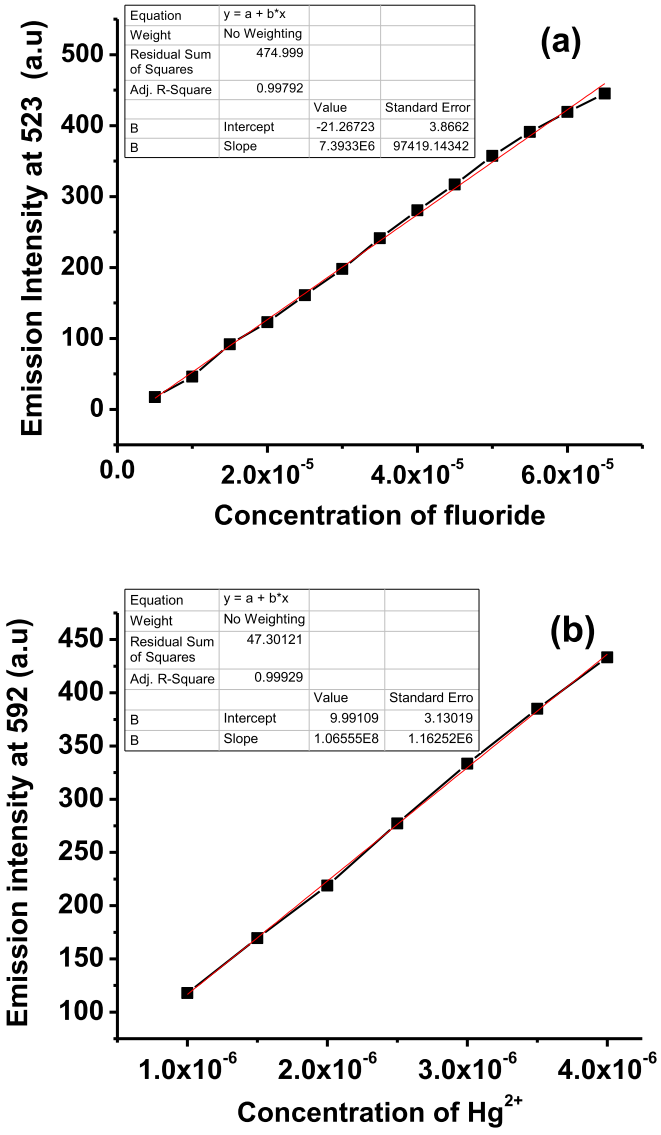

Fig. 5. Linear response curves of **1** at 523 nm depending on the F^- (a) and at 592 nm depending on the Hg^{2+} (b) concentration.

characteristics of **1** presented in Figs S8–S9, Supporting data, complement each other. The lower detection limit of the probe in the case of $F^-$and Hg^{2+} was calculated from fluorescence linear response curves (Fig. 5) using the formula, Detection limit = K (SD)/S, Where $K = 2$ or 3, we take 3 in this case. 'SD' is the standard deviation of the blank solution, 'S' is the slope of the calibration curve. The standard deviation of blank in the case of F^- and Hg^{2+} is 0.1274 and 0.1918, respectively. The calculated detection limits of the probe are 5.17×10^{-8} M (~1.0 ppb) and 5.4×10^{-9} M (~1.1 ppb), respectively for F^- and Hg^{2+} in aqueous samples.

In order to confirm the non-interference of other metal ions and anions, competition experiments were performed in the presence of excess concentrations of other commonly coexisting ions (Figs. S10a and S10b, Supporting data) and the results suggested that **1** can detect F^- and Hg^{2+} even in the presence of excess concentrations of other competitive metal ions. After establishing the non-interference of other ions, it was imperative to explore the effect of Hg^{2+} ions in the detection of F^- ions, and *vice versa*. The excitation and emission spectra of **1** with Hg^{2+} or/and F^- ions, in isolation and in combination were recorded. Addition of thirty equivalents of F^- ions (150 μM) to the non-fluorescent probe **1** (5 μM) showed the maximum level of absorption at ~500 nm and fluorescence emission at ~523 nm (Fig. 6). When metal ions such as Na^+, K^+, Ca^{2+}, Mg^{2+}, Cr^{3+}, Cu^{2+}, Fe^{3+}, Co^{2+}, Mn^{2+}, Cd^{2+}, Zn^{2+}, Pb^{2+} and Ni^{2+} were added (15 μM) to the above solution, neither the absorption nor the fluorescence profile of the solution was affected. However, addition of Hg^{2+} (15 μM) produced a new absorption peak at ~568 nm, in addition to an increase in the intensity of absorption band at ~500 nm (Fig. 6a). While the appearance of the new peak at ~568 nm could be attributed to the formation of **4** ($m/z = 812$, Fig. S11, Supporting data) with spirolactam ring opened rhodamine moiety (Scheme S1, Supporting data), the increase in intensity of absorption at ~500 nm was ascribed to spectral overlap. Under comparable conditions, the fluorescence emission at ~523 nm of **2** [obtained from **1** (5 μM) and 30 equivalents of F^-] was diminished to the basal level, and a new emission band centered at ~592 nm appeared (Fig. 6b) upon addition of Hg^{2+} (15 μM), presumably due to the intramolecular FRET from fluorescein moiety (donor) to rhodamine moiety (acceptor) in **4**. However, the observed intensity of the emission band centered at ~592 nm, obtained by the addition of only Hg^{2+} ions (15 μM) to probe **1** (5 μM), was lower than that observed with the combined addition of F^- (150 μM) and Hg^{2+} (15 μM) to probe **1** (5 μM) (Fig. S12, Supporting data). This difference in emission intensity could be explained by the intramolecular FRET between the fluoresceine and rhodamine

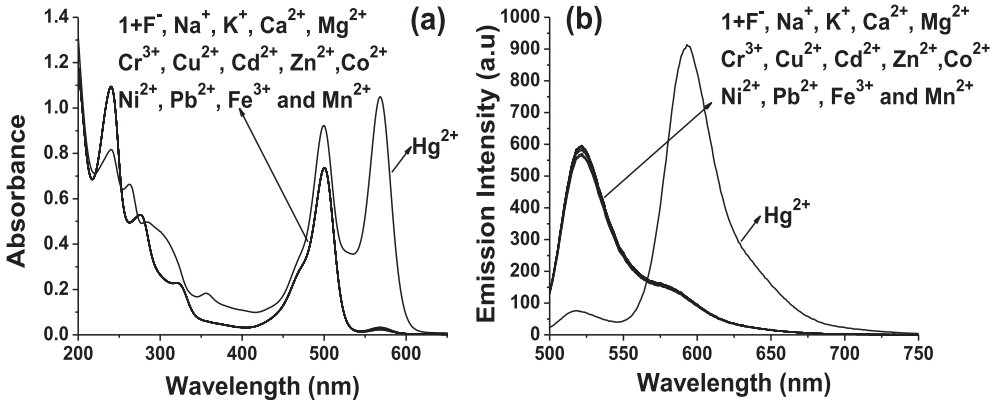

Fig. 6. Metal ion (15 μM) induced variations in the (a) absorbance, and (b) fluorescence spectra of **2** [obtained from **1** (5 μM) and 30 equivalents of F^-]; Excitation wavelength: 480 nm.

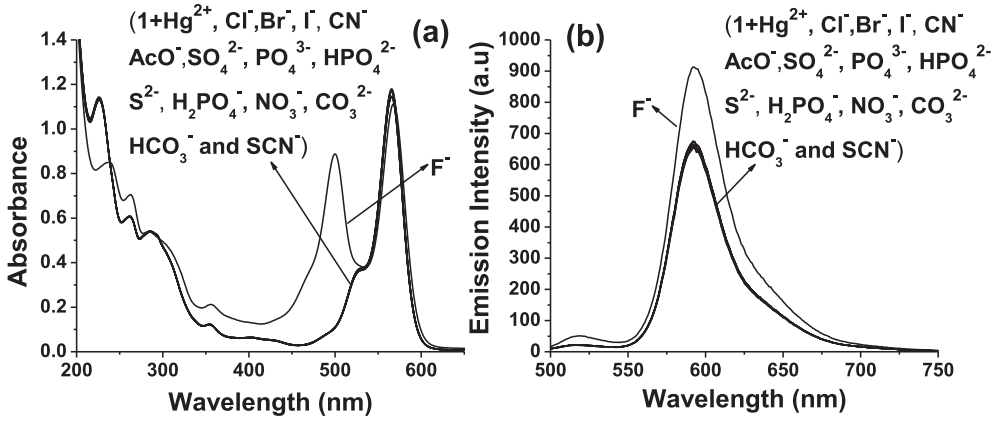

Fig. 7. Anion (150 μM) induced variations in the (a) absorbance, and (b) fluorescence spectra of **3** [obtained from **1** (5 μM) and 3 equivalents of Hg^{2+}]; Excitation wavelength: 480 nm.

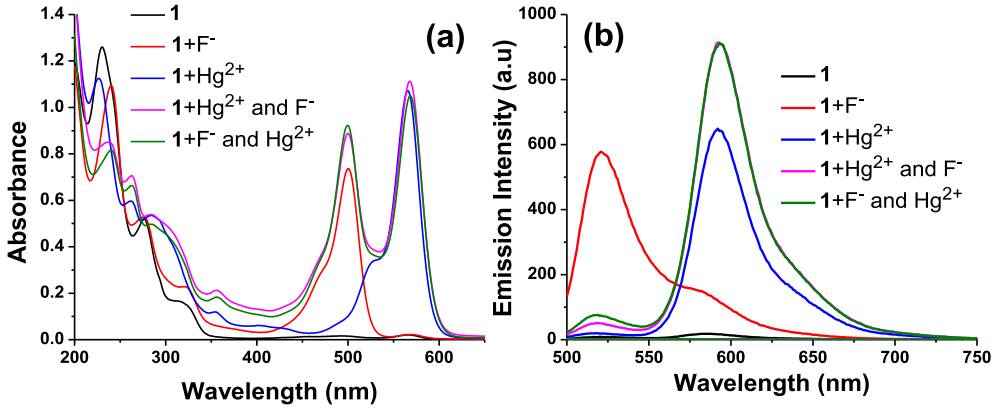

Fig. 8. Absorption (a) and emission (b) profiles of probe **1** (5 μM) in 1:1 v/v 0.01 M Tris HCl–CH_3CN, pH 7.4 in response to the addition of fluoride (150 μM) and Hg^{2+} (15 μM) ions, individually and collectively. Excitation wavelength: 480 nm.

moieties. Similarly, addition of only F^- (150 μM) to the solution of **3** [obtained from **1** (5 μM) and 3 equivalents of Hg^{2+}] selectively developed an absorption band at ~500 nm (Fig. 7a), and enhanced the emission intensity at ~592 nm (Fig. 7b). These observations could be attributed to the F^- selective cleavage of Si–O linkage leading to the opening of fluorescein spirocyclic ring, and subsequently, the FRET form fluorescein moiety to rhodamine moiety. Thus, the absorption and fluorescence profiles displayed by probe **1** to the addition of F^- and Hg^{2+} ions appear to permit the selective detection of F^- and Hg^{2+} in isolation and in combination. The effect of collective addition of F^- and Hg^{2+} to **1** (Fig. 8) also corroborated the above mentioned observations (Figs. 1–4 and 6,7).

Careful analysis of Figs. 6–8, revealed the possibility of ratiometric detection of F^- in absorption mode and that of Hg^{2+} in fluorescence mode. For the ratiometric detection of F^- in absorption mode, compound **3** (Scheme S1, Supporting data) was first

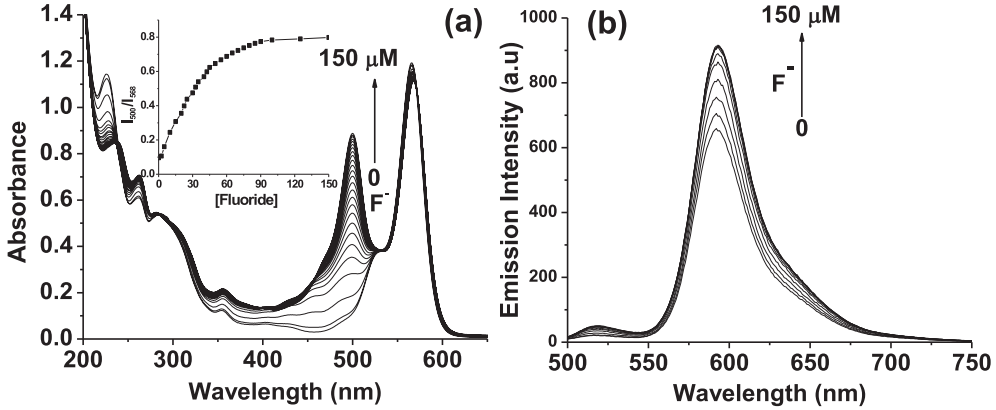

Fig. 9. Ratiometric titration: Fluoride (0–150 μM) induced variations in the absorption (a) and emission spectra (b) of **3** (obtained from **1** (5 μM) and 3 equivalents of Hg^{2+}) in 1:1 v/v 0.01 M Tris HCl–CH_3CN, pH 7.4. Excitation wavelength was 480 nm. Inset to a: plot of I_{500}/I_{568} *versus* [F^-].

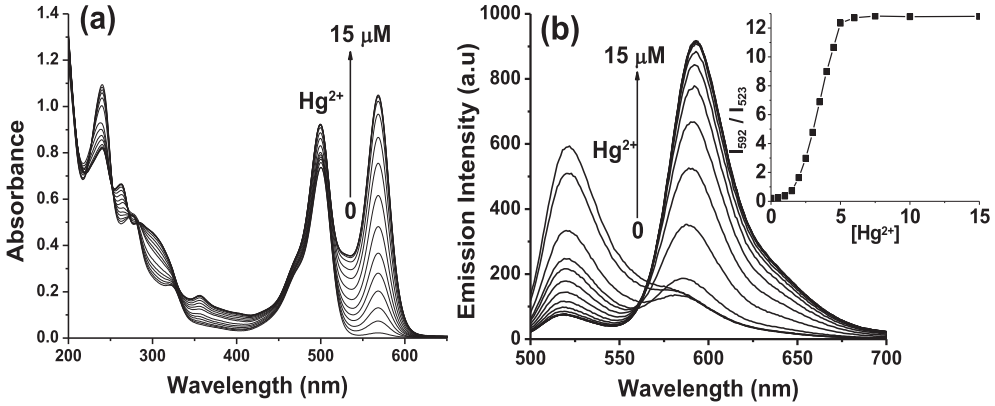

Fig. 10. Ratiometric titration: Hg^{2+} (0–15 μM) induced variations in the absorption (a) and emission spectra (b) of **2** (obtained from 5 μM of **1** and 30 equivalents of F^-) in 1:1 v/v 0.01 M Tris HCl–CH_3CN, pH 7.4. Excitation wavelength: 480 nm. Inset to b: plot of the ratio of the emission intensity at 592 nm and 523 nm vs concentration of Hg^{2+}.

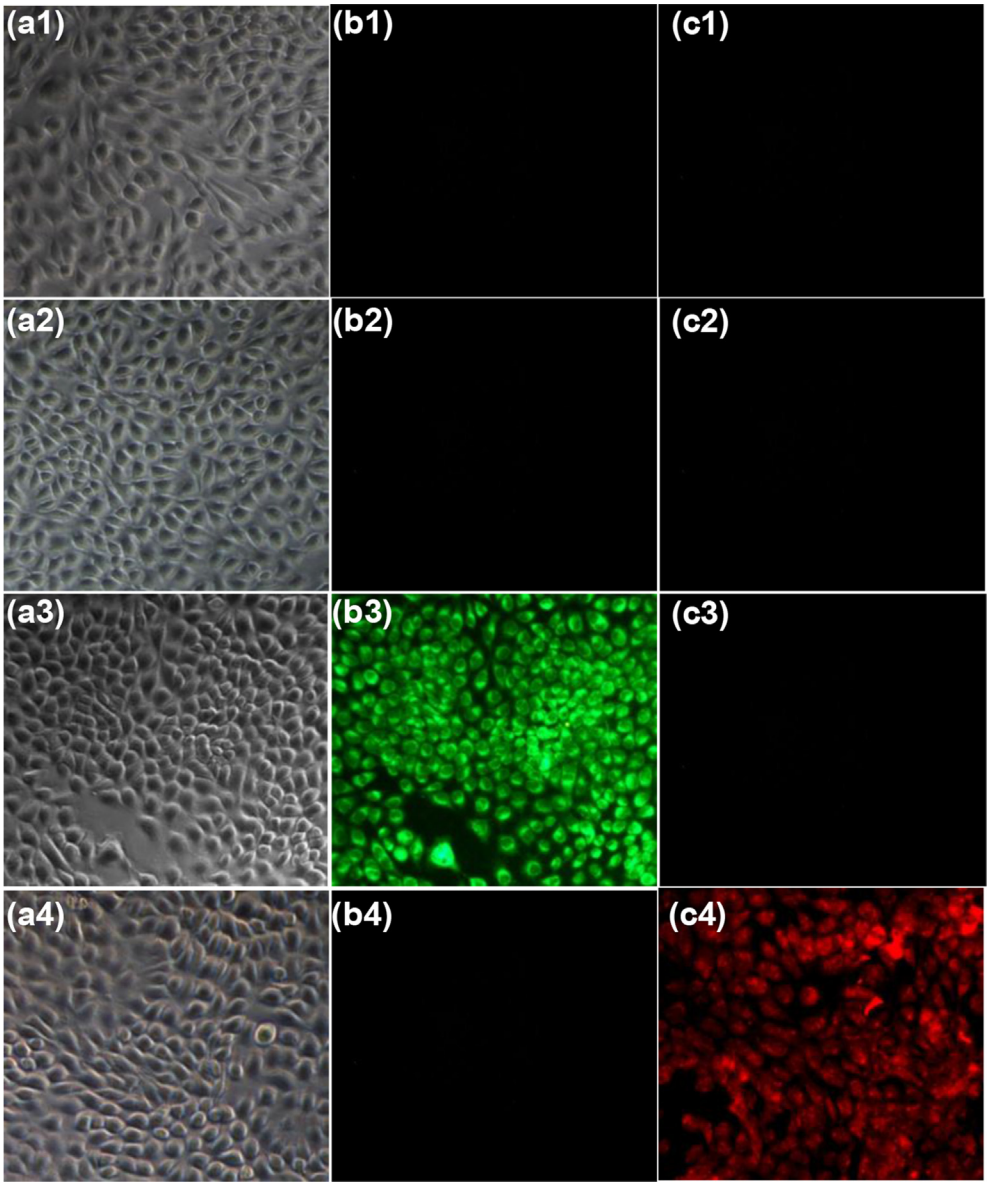

Fig. 11. Fluorescence microscopic images of W138 normal lung fibroblast cells: Row 1 (a1–c1): untreated cells, Row 2 (a2–c2): cells treated with **1** (5 μM) alone; Row 3 (a3–c3): cells treated with **1** (5 μM) and F^- (50 μM); Row 4 (a4–c4): cells treated with **1** (5 μM) and Hg^{2+} (5 μM); Column 1 (a1–a4), bright field images; Column 2 (b1–b4), fluorescence images obtained using green filter; Column 3 (c1–c4), fluorescence images obtained using red filter. (For interpretation of the references to colour in this figure legend, the reader is referred to the web version of this article.)

obtained by reacting probe **1** (5 μM) with Hg^{2+} ions (15 μM). The UV–visible spectrum of this solution showed an absorption band at ~568 nm. Progressive addition of serial concentrations of F^- ions produced a new absorption band at ~500 nm with a gradual increase in its intensity, as seen in Fig. 9a. The ratio of absorption intensities I_{500}/I_{568} for a given concentration of F^- ions permitted the ratiometric detection. The calculated detection limit was 1.8×10^{-7} M (~3.24 ppb) (Fig. S13a, Supporting data). For the ratiometric detection of Hg^{2+} in fluorescence mode, compound **2** (Scheme S1, Supporting data) was obtained by reacting probe **1** (5 μM) with F^- ions (150 μM), and its fluorescence spectrum was recorded. Addition of Hg^{2+} resulted in a new emission band at ~592 nm (Fig. 10b) whose intensity was proportional to the amount of Hg^{2+} added. Addition of increasing amounts of Hg^{2+} also resulted in progressive reduction in the intensity of emission at ~523 nm, and thereby, allowed the ratiometric detection of Hg^{2+} ions (Inset to Fig. 10b). The calculated detection limit was 4.8×10^{-9} M (~1 ppb) (Fig. S13b, Supporting data).

To explore the potential of the probe **1** in the imaging of live cells, its cytotoxicity to NIH 3T3 cells was estimated using MTT assay. The observed cell viability (Fig. S14, Supporting data) suggested that the non-lethal concentration range of **1** was up to 10 μM. The effect of pH on the fluorescence emission pattern of **1** was evaluated using acid-base titration experiments [38–44]. The fluorescence profile of **1** remains unchanged in the pH range from pH 5.0 to 10 (Fig. S15, Supporting data). The results indicated that the probe is stable over a broad pH range, and confirmed that the observed changes in the fluorescence or absorbance profiles of **1** upon addition of analytes (F^- and Hg^{2+}) are solely due to the interaction between the probe and the analyte(s). The non-cytotoxic nature of **1**, stability at physiological pH 7.4 and non-interference of other cations and anions in the simultaneous detection of Hg^{2+} and F^-, paved the way for the detection of these toxic ions present in contaminated live cells. The imaging of live cells exposed to F^- and Hg^{2+} was carried out using only 5 μM concentration of **1** (Fig. 11). The bright field and fluorescence microscopic images of the cells alone (row 1), cells loaded with **1** alone (row 2), cells loaded with **1** and then treated with F^- (row 3), and cells loaded with **1** and then treated with Hg^{2+} (row 4) are shown in Fig. 11.

The fluorescence images obtained using the green channel (column 2) and the red channel (column 3) showed that the cells alone and cells loaded with **1** (5 μM) were non-fluorescent. However, incubation with F^- ions (50 μM) for 15 min at 37 °C enabled the probe loaded cells to emit an intense green fluorescence in the green channel (column 2, row 3), presumably from the in situ generated fluorophore **2**. The absence of red fluorescence in the red channel (column 3, row 3) indicated that the rhodamine moiety in **2** (Scheme S1, Supporting data) existed in the ring-closed spirolactam form. Under identical conditions, cells loaded with **1** and incubated with Hg^{2+} (5 μM) for 15 min at 37 °C displayed an intense red fluorescence (column 3, row 4) apparently from the spirolactam ring-open form of rhodamine moiety in **3** (Scheme S1, Supporting data). These results clearly demonstrated the suitability of probe **1** for the detection of intracellular F^- and Hg^{2+} ions.

4. Conclusion

In conclusion, based on two fluorophore embedded approach, we have developed a new fluorescein-rhodamine conjugate **1** useful for the simultaneous detection of both F^- and Hg^{2+} ions selectively even in the presence of competitive ions. The versatility of the probe **1** to transform into **2**, **3** and **4** with respect to the presence of F^- and Hg^{2+} in isolation and in combination permits both linear and ratiometric detection of these ions at ppb levels. Fluoride and Hg^{2+} specific optical and fluorescence responses of **1** preclude interference by other competitive ions, and thereby, overcome the main drawback encountered by other multi-analyte probes reported in the literature. Further, the probe **1** is cell membrane permeable, stable at physiological pH and non-lethal under the experimental conditions, and hence, could be used for the detection and imaging of W138 normal lung fibroblast cells contaminated with F^- and Hg^{2+} ions. We hope that the two fluorophore embedded approach demonstrated in this communication will help augment the design and development of new multi-analyte probes.

Acknowledgments

N. R. Ch. thanks the CSIR, India, for CSIR-Nehru Science Post-doctoral Fellowship. P. N. thanks the CSIR, India, for research fellowship. Financial support from CSIR 12th plan project CSC0201 and INTELCOAT is acknowledged.

Appendix A. Supplementary data

Supplementary data related to this article can be found at http://dx.doi.org/10.1016/j.dyepig.2014.07.004.

References

[1] Chen X, Pradhan T, Wang F, Kim JS, Yoon J. Fluorescent chemosensors based on spiroring-opening of xanthenes and related derivatives. Chem Rev 2012;112:1910–56.
[2] Zheng H, Zhan X-Q, Bian Q-N, Zhang X-J. Advances in modifying fluorescein and rhodamine fluorophores as fluorescent chemosensors. Chem Commun 2013;49:429–47.
[3] Li X, Gao X, Shi W, Ma H. Design strategies for water-soluble small molecular chromogenic and fluorogenic probes. Chem Rev 2014;114:590–659.
[4] Gutknecht J. Inorganic mercury (Hg^{2+}) transport through lipid bilayer membranes. J Membr Biol 1981;61:61–6.
[5] Horowitz HS. The 2001 CDC recommendations for using fluoride to prevent and control dental caries in the United States. J Public Health Dent 2003;63:3–8.
[6] Farley JR, Wergedal JE, Baylink DJ. Fluoride directly stimulates proliferation and alkaline phosphatase activity of bone-forming cells. Science 1983;222:330–2.
[7] Kleerekoper M. The role of fluoride in the prevention of osteoporosis. Endocrinol Metab Clin North Am 1998;27:441–52.
[8] Wiseman A. Handbook of experimental pharmacology, vol. XX/2 Part 2. Berlin: Springer; 1970.
[9] Dreisbuch RH. Handbook of poisoning. Los Altos, CA: Lange Medical Publishers; 1980.
[10] Gessner BD, Beller M, Middaugh JP, Whitford GM. Acute fluoride poisoning from a public water system. N Engl J Med 1994;330:95–9.
[11] Liu B, Tian H. A selective fluorescent ratiometric chemodosimeter for mercury ion. Chem Commun 2005:3156–8.
[12] Shiraishi Y, Sumiya S, Hirai T. A coumarin–thiourea conjugate as a fluorescent probe for Hg(II) in aqueous media with a broad pH range 2–12. Org Biomol Chem 2010;8:1310–4.
[13] Lee MH, Lee SW, Kim SH, Kang C, Kim JS. Nanomolar Hg(II) detection using Nile blue chemodosimeter in biological media. Org Lett 2009;11:2101–4.
[14] Guo Z, Zhu W, Zhu M, Wu X, Tian H. Near-infrared cell-permeable Hg^{2+}-selective ratiometric fluorescent chemodosimeters and fast indicator paper for $MeHg^+$ based on tricarbocyanines. Chem Eur J 2010;16:14424–32.
[15] Shang G-Q, Gao X, Chen M-X, Zheng H, Xu J-G. A novel Hg^{2+} selective ratiometric fluorescent chemodosimeter based on an intramolecular FRET mechanism. J Fluoresc 2008;18:1187–92.
[16] Yang Y-K, Yook K-J, Tae J. A rhodamine-based fluorescent and colorimetric chemodosimeter for the rapid detection of Hg^{2+} ions in aqueous media. J Am Chem Soc 2005;127:16760–1.
[17] Wu JS, Hwang IC, Kim KS, Kim JS. Rhodamine-based Hg^{2+}-selective chemodosimeter in aqueous solution: fluorescent OFF-ON. Org Lett 2007;9:907–10.
[18] Zhang X, Xiao Y, Qian X. A ratiometric fluorescent probe based on FRET for imaging Hg^{2+} ions in living cells. Angew Chem Int Ed 2008;47:8025–9.
[19] Wang F, Nam S-W, Guo Z, Park S, Yoon J. A new rhodamine derivative bearing benzothiazole and thiocarbonyl moieties as a highly selective fluorescent and colorimetric chemodosimeter for Hg^{2+}. Sens Actuators B 2012;161:948–53.
[20] Kim SY, Hong J-I. Chromogenic and fluorescent chemodosimeter for detection of fluoride in aqueous solution. Org Lett 2007;9:3109–12.
[21] Bozdemir OA, Sozmen F, Buyukcakir O, Guliyev R, Cakmak Y, Akkaya EU. Reaction-based sensing of fluoride ions using built-in triggers for

intramolecular charge transfer and photoinduced electron Transfer. Org Lett 2010;12:1400–3.
[22] Zhang JF, Lim CS, Bhuniya S, Cho BR, Kim JS. A highly selective colorimetric and ratiometric two-photon fluorescent probe for fluoride ion detection. Org Lett 2011;13:1190–3.
[23] Hu R, Feng J, Hu D, Wang S, Li S, Li Y, et al. A rapid aqueous fluoride ion sensor with dual output modes. Angew Chem Int Ed 2010;49:4915–8.
[24] Zhu B, Yuan F, Li R, Li Y, Wei Q, Ma Z, et al. A highly selective colorimetric and ratiometric fluorescent chemodosimeter for imaging fluoride ions in living cells. Chem Commun 2011;47:7098–100.
[25] Zheng F, Zeng F, Yu C, Hou X, Wu S. A PEGylated fluorescent turn-on sensor for detecting fluoride ions in totally aqueous media and its imaging in live cells. Chem Eur J 2013;19:936–42.
[26] Guo Z, Song NR, Moon JH, Kim M, Jun EJ, Choi J, et al. A benzobisimidazolium-based fluorescent and colorimetric chemosensor for CO_2. J Am Chem Soc 2012;134:17846–9.
[27] Yuan M, Zhou W, Liu X, Zhu M, Li J, Yin X, et al. A multianalyte chemosensor on a single molecule: promising structure for an integrated logic gate. J Org Chem 2008;73:5008–14.
[28] He X, Yam VW-W. A highly selective bifunctional luminescence probe for potassium and fluoride ions. Org Lett 2011;13:2172–5.
[29] Paramanik B, Bhattacharyya S, Patra A. Detection of Hg^{2+} and F^- ions by using fluorescence switching of quantum dots in an Au-cluster–CdTe QD nanocomposite. Chem Eur J 2013;19:5980–7.
[30] Kumari N, Dey N, Bhattacharya S. Rhodamine based dual probes for selective detection of mercury and fluoride ions in water using two mutually independent sensing pathways. Analyst 2014;139:2370–8.
[31] Kumar M, Kumar R, Bhalla V. A reversible fluorescent Hg^{2+}/K^+ switch that works as keypad lock in the presence of F^- ion. Chem Commun 2009:7384–6.
[32] Sutariya PG, Modi NR, Pandya A, Joshi BK, Joshi KV, Menon SK. An ICT based "turn on/off" quinoline armed calix[4]arenefluoroionophore: its sensing efficiency towards fluoride from waste water and Zn^{2+} from blood serum. Analyst 2012;137:5491–4.
[33] Suresh M, Ghosh A, Das A. A simple chemosensor for Hg^{2+} and Cu^{2+} that works as a molecular keypad lock. Chem Commun 2008:3906–8.
[34] Maity D, Govindaraju T. A differentially selective sensor with fluorescence turn-on response to Zn^{2+} and dual-mode ratiometric response to Al^{3+} in aqueous media. Chem Commun 2012;48:1039–41.
[35] Basa PN, Sykes AG. Differential sensing of Zn(II) and Cu(II) via two independent mechanisms. J Org Chem 2012;77:8428–34.
[36] Karakus E, Ucuncu M, Emrullahoglu M. A rhodamine/BODIPY-based fluorescent probe for the differential detection of Hg(II) and Au(III). Chem Commun 2014;50:1119–21.
[37] Xu Z, Kim S, Kim HN, Han SJ, Lee C, Kim JS, et al. A naphthalimide–calixarene as a two-faced and highly selective fluorescent chemosensor for Cu^{2+} or F^-. Tetrahedron Lett 2007;48:9151–4.
[38] Chereddy NR, Thennarasu S. Synthesis of a highly selective bis-rhodaminechemosensor for naked-eye detection of Cu^{2+} ions and its application in bio-imaging. Dyes Pigments 2011;91:378–82.
[39] Chereddy NR, Thennarasu S, Mandal AB. A new triazole appended rhodamine chemosensor for selective detection of Cu^{2+} ions and live-cell imaging. Sens Actuators B 2012;171–172:294–301.
[40] Chereddy NR, Janakipriya S, Korrapati PS, Thennarasu S, Mandal AB. Solvent-assisted selective detection of sub-micromolar levels of Cu^{2+} ions in aqueous samples and live-cells. Analyst 2013;138:1130–6.
[41] Chereddy NR, Thennarasu S, Mandal AB. Incorporation of triazole into a quinoline-rhodamine conjugate imparts iron(III) selective complexation permitting detection at nanomolar levels. Dalt Trans 2012;41:11753–9.
[42] Chereddy NR, Thennarasu S, Mandal AB. A highly selective and efficient single molecular FRET based sensor for ratiometric detection of Fe^{3+} ions. Analyst 2013;138:1334–7.
[43] Chereddy NR, Suman K, Korrapati PS, Thennarasu S, Mandal AB. Design and synthesis of rhodamine based chemosensors for the detection of Fe^{3+} ions. Dyes Pigments 2012;95:606–13.
[44] Chereddy NR, Korrapati PS, Thennarasu S, Mandal AB. Tuning copper(II) ion selectivity: the role of basicity, size of the chelating ring and orientation of coordinating atoms. Dalt Trans 2013;42:12873–7.
[45] Goswami S, Aich K, Das S, Das AK, Sarkar D, Panja S, et al. A red fluorescence 'off-on' molecular switch for selective detection of Al^{3+}, Fe^{3+} and Cr^{3+}: experimental and theoretical studies along with living cell imaging. Chem Commun 2013;49:10739–41.